Biomaterials 287 (2022) 121643

Contents lists available at ScienceDirect

Biomaterials

journal homepage: www.elsevier.com/locate/biomaterials

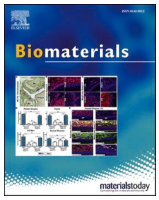

Empowering engineered muscle in biohybrid pump by extending connexin 43 duration with reduced graphene oxides

Eunkyung Ko [a,b,d], Onur Aydin [c], Zhengwei Li [c], Lauren Gapinske [a,b], Kai-Yu Huang [f], Taher Saif [c], Rashid Bashir [a,b,d,e,**], Hyunjoon Kong [a,d,e,f,g,*]

[a] Department of Bioengineering, University of Illinois at Urbana-Champaign, Urbana, IL 61801, USA
[b] Micro and Nanotechnology Laboratory, University of Illinois at Urbana-Champaign, Urbana, IL 61801, USA
[c] Department of Mechanical Science and Engineering, University of Illinois at Urbana-Champaign, Urbana, IL 61801, USA
[d] Carl R. Woese Institute for Genomic Biology, University of Illinois at Urbana-Champaign, Urbana, IL, USA
[e] Beckman Institute for Advanced Science and Technology, University of Illinois at Urbana-Champaign, Urbana, IL, USA
[f] Department of Chemical and Biomolecular Engineering, University of Illinois at Urbana-Champaign, Urbana, IL 61801, USA
[g] KU-KIST Graduate School of Converging Science and Technology, Korea University, Seongbuk-gu, Seoul 02841, South Korea

ARTICLE INFO

Keywords:
Reduced graphene oxide
Gap junction protein
Connexin 43
Skeletal muscle
Biohybrid pump
Troponin

ABSTRACT

Engineered skeletal muscle act as therapeutics invaluable to treat injured or diseased muscle and a "living" material essential to assemble biological machinery. For normal development, skeletal myoblasts should express connexin 43, one of the gap junction proteins that promote myoblast fusion and myogenesis, during the early differentiation stage. However, myoblasts cultured in vitro often down-regulate connexin 43 before differentiation, limiting myogenesis and muscle contraction. This study demonstrates that tethering myoblasts with reduced graphene oxide (rGO) slows connexin 43 regression during early differentiation and increases myogenic mRNA synthesis. The whole RNA sequencing also confirms that the rGO on cells increases regulator genes for myogenesis, including troponin, while decreasing negative regulator genes. The resulting myotubes generated a three-fold larger contraction force than the rGO-free myotubes. Accordingly, a valveless biohybrid pump assembled with the rGO-tethered muscle increased the fluid velocity and flow rate considerably. The results of this study would provide an important foundation for developing physiologically relevant muscle and powering up biomachines that will be used for various bioscience studies and unexplored applications.

1. Introduction

The development of a reliable in vitro skeletal muscle model system has the potential to benefit both fundamental and applied bioscience studies. For instance, skeletal muscle recreated with patients' stem or precursor cells can simulate development, regeneration, and pathogenesis and screen newly developed therapeutics. The engineered muscle may also be transplanted to treat acute muscle injuries and chronic skeletal degenerative diseases [1,2]. Recent studies have used engineered muscle to power biological machines capable of locomotion and performing desired functions [3–6]. Success relies on the ability to reproduce muscle with physiologically relevant contraction force. However, the engineered skeletal muscle generates the force usually in micronewton scale, which is smaller than in vivo muscle.

Various approaches have been made to enhance force generation by exercising the engineered muscle or adding growth factors or small molecules during maturation [7–9]. Recently, the early loss of gap junction protein during myogenic differentiation has been brought to attention as a limiting factor. Gap junctions connect neighboring cells and allow intercellular transports of ions, electrical signals, and small metabolic molecules [10–14]. Among the gap junction proteins, connexin 43 is abundant in cardiomyocytes and skeletal myoblasts [15,16]. The connexin 43 promotes intercellular association during myogenesis and propagates action potential signals through the cells, leading to synchronized muscle contraction [17,18]. It has also been reported that connexin 43 may contribute to muscle tissue regeneration [19].

* Corresponding author. Department of Chemical and Biomolecular Engineering, University of Illinois at Urbana-Champaign Urbana, IL 61801, USA.
** Corresponding author. College of Engineering Grainger Distinguished Chair in Engineering, Professor of Bioengineering, University of Illinois at Urbana-Champaign 306 Engineering Hall, MC-266 1308 W. Green Street, Urbana, IL 61801, USA.
E-mail addresses: rbashir@illinois.edu (R. Bashir), hjkong06@illinois.edu (H. Kong).

https://doi.org/10.1016/j.biomaterials.2022.121643
Received 24 January 2022; Received in revised form 8 June 2022; Accepted 17 June 2022
Available online 24 June 2022

Conversely, suppression of connexin 43 in mice impact skeletal muscle development, as evidenced by reduced muscle weight.

Graphene-based materials have been widely used in skeletal muscle engineering for the past decade due to their, mechanical, and electrical properties. For example, studies have shown that graphene-based materials are known to provide microenvironments that support cell adhesion and proliferation [20,21]. In general, the functional groups (i.e. hydroxyl, carboxyl, carbonyl, and carboxylate groups) on the surface of the graphene enhance electrostatic, covalent, and hydrogen bondings which subsequently promote the adhesiveness of cells [20]. Furthermore, graphene-based materials mixed with polymers including alginate, collagen, and gelatin can support myogenic differentiation [22–24].

Cardiomyocytes retain connexin 43 from the early to late differentiation stage. Skeletal myoblasts also present connexin 43 during the early differentiation in vivo [17,19]. However, they undergo downregulation after cells fuse to form myotubes. Then, motor neurons innervating myotubes take over control of muscle contraction [16,25]. In contrary, skeletal myoblasts cultured in vitro undertake early connexin 43 downregulation even before myogenic differentiation initiates, leading to limited myofiber formation and contraction.

To resolve this challenge, this study hypothesizes that reduced graphene oxide (rGO) flakes tethered to myoblasts would extend the duration of connexin 43 and subsequently recreate muscle with increased contraction frequency and force. In particular, rGO anchored on cells would promote the adsorption of extracellular matrix (ECM) proteins, which would support the assembly of connexin 43 into gap junctions between cells [26,27]. In this study, we tethered rGO to C2C12 skeletal myoblasts, a model muscle precursor cell (Fig. 1A). The tethered cells were collected to evaluate myogenic differentiation both in 2D and 3D. We first examined the extent to which rGO sustains cellular connexin 43 expressions and enhances myogenic differentiation by conducting immunofluorescence staining and quantitative real-time polymerase chain reaction (qRT-PCR) at different stages of differentiation. We also performed the whole RNA-sequencing to observe transcriptional activities. Lastly, we tested if the extended connexin 43 expression powers up 3D muscle contraction using a biohybrid Pump-Bot. This biological robot was designed to recapitulates the blood circulation mechanism in an embryonic vertebrate heart [6]. This study provides a new insight into the use of rGO for retention of connexin 43

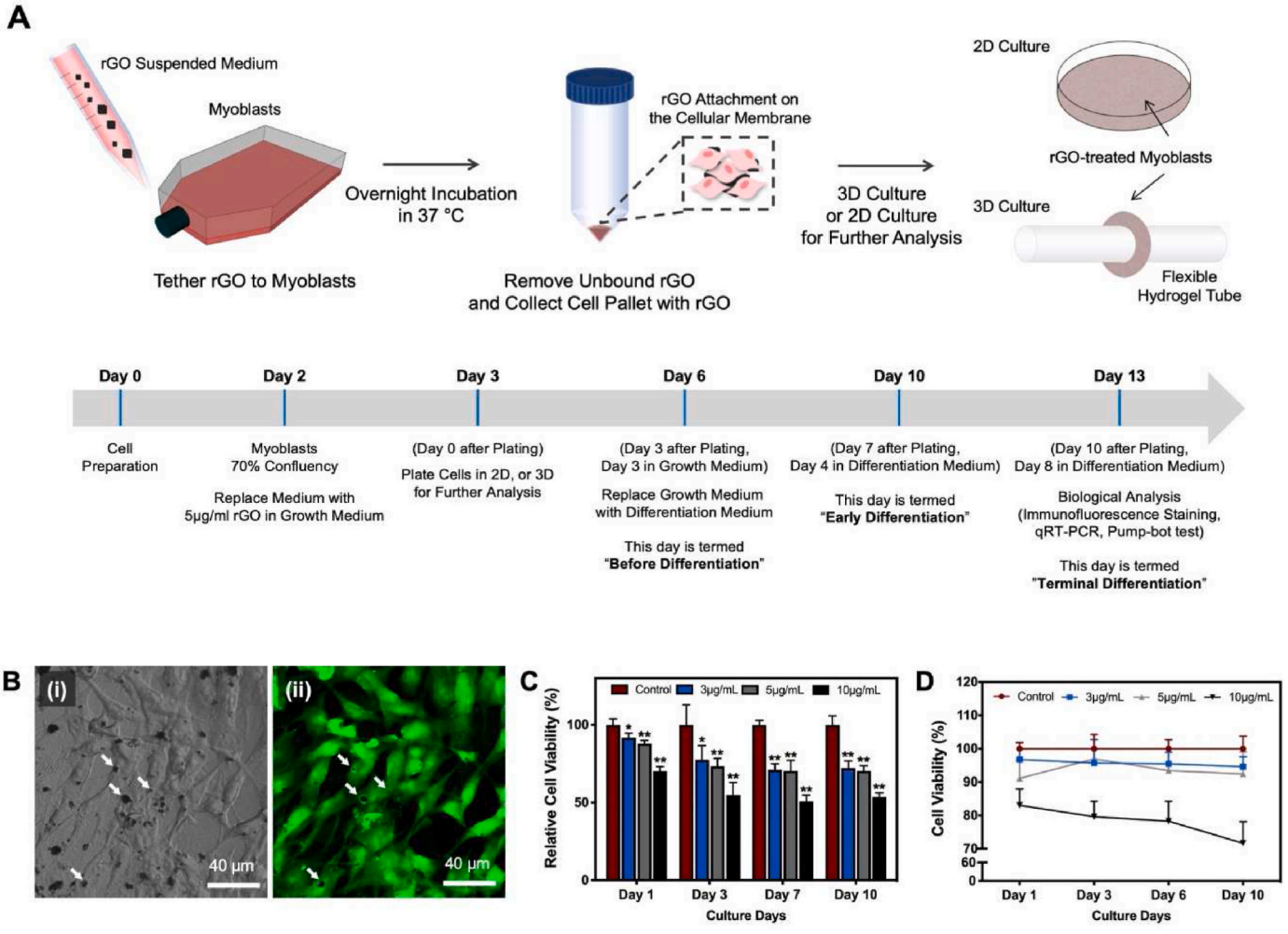

Fig. 1. Tethering rGO flakes to skeletal myoblasts. (A) Procedure to prepare and analyze engineered muscle tethered with rGO. Myoblasts are first incubated in the rGO flakes-suspending medium overnight at 37 °C. The next day, cells tethered with rGO flakes are collected and used to prepare a monolayer cell sheet or a 3D muscle ring. The growth medium is replaced with a myogenic differentiation medium on day 3. After 7 days, the quality of engineered muscle was evaluated by examining genomic patterns, phenotypes, and contraction. **(B)** (i) Optical image of the myoblast tethered with rGO flakes. (ii) Fluorescently quenched rGO flakes on cells. In this image, the cell membrane was labeled with fluorescein. The white arrows indicate representative quenched areas. (C, D) Viability of myoblasts tethered with different concentrations of rGO tested by Trypan blue staining (C) and Live/Dead assay (D). Each bar value and error bar represent the average and standard deviation of four different samples per condition (*$p < 0.05$, **$p < 0.01$). (For interpretation of the references to color in this figure legend, the reader is referred to the Web version of this article.)

and enhanced myogenic differentiation.

2. Results and discussion

2.1. rGO flakes adhere to cell surface with minimal internalization

First, we incubated myoblasts with rGO flakes with an average length of 5 μm and width of 4 μm, as shown with the transmission electron microscopy image (Supporting InformationFigure S1A). Within 12 h s, rGO adhered to myoblasts stably. The Raman spectrum of the rGO on cells showed two distinct peaks, known as the *G* and *D* bands (Supporting Information Figure S1B). Centrifugation removed unbound rGO flakes while keeping rGO flakes tethered to the cell surface, as shown with brightfield images (Fig. 1B(i)). We reconfirmed the rGO bound to the cell surface by photo-bleaching fluorescein associated with rGO (Fig. 1B(ii)). According to the quantification made with photo-bleached images, about 1% of the cell surface was covered with rGO flakes. No flakes were found within cells, indicating that cells did not take up the micro-sized rGO flakes.

We also evaluated the cytotoxicity of rGO to myoblasts by incubating cells in the media, suspending controlled concentrations of rGO flakes, counting the number of dead cells stained for Trypan blue, and performing a Live/Dead assay (Fig. 1C and D, and Supporting InformationFigure S2). According to the number of cells counted with Trypan blue staining at different time points, more than 80% of cells remained viable with 3 and 5 μg/ml rGO flakes until day 10. The cells incubated with 10 μg/ml rGO flakes also showed above 70% survival rate until day 10.

According to the International Organization for Standardization, materials that keep cell viability at a level higher than 70% are considered biocompatible (10,993-5) [28]. In contrast, the fraction of viable myoblasts incubated with 10 μg/ml rGO was dropped to 70% within 24 h s. Therefore, the following studies kept the concentration of the rGO flakes in the incubation media at 5 μg/ml. At this concentration, cells minimally internalized the micro-sized rGO flakes.

2.2. rGO flakes tethered to myoblasts extend duration of connexin 43 expressions

Cellular connexin 43 expressions were analyzed by performing immunofluorescence imaging on day 3 (before differentiation), day 7 (early differentiation), and day 13 (terminal differentiation) (Fig. 2A). We compared connexin 43 expressions of the rGO-tethered myoblasts with untreated ones. In both groups, connexin 43 was visible before differentiation. However, the untreated myoblasts lost connexin 43 expressions after they started differentiation. In contrast, rGO-tethered myoblasts continued to express connexin 43 during the early differentiation stage. The expression was finally downregulated at the terminal differentiation stage.

We additionally performed qRT-PCR to quantify the relative connexin 43 mRNA expression level. We used the result to plot two graphs to compare the connexin 43 expression level between untreated myoblasts and rGO-tethered myoblasts at different time points and how connexin expression was changed in each group over time. The connexin 43 mRNA expression level of rGO-tethered myoblasts was 1.2-fold higher on day 3, 1.4-fold higher on day 7, and 1.2-fold higher on day 13 than untreated group (Fig. 2B). We also confirmed that connexin 43 mRNA expression was downregulated more rapidly in untreated myoblasts than rGO-tethered myoblasts (Fig. 2C).

2.3. rGO flakes bound to myoblasts enhance myotube formation

We tested if the rGO flakes tethered to myoblasts enhance myogenic differentiation by performing immunofluorescence imaging and qRT-

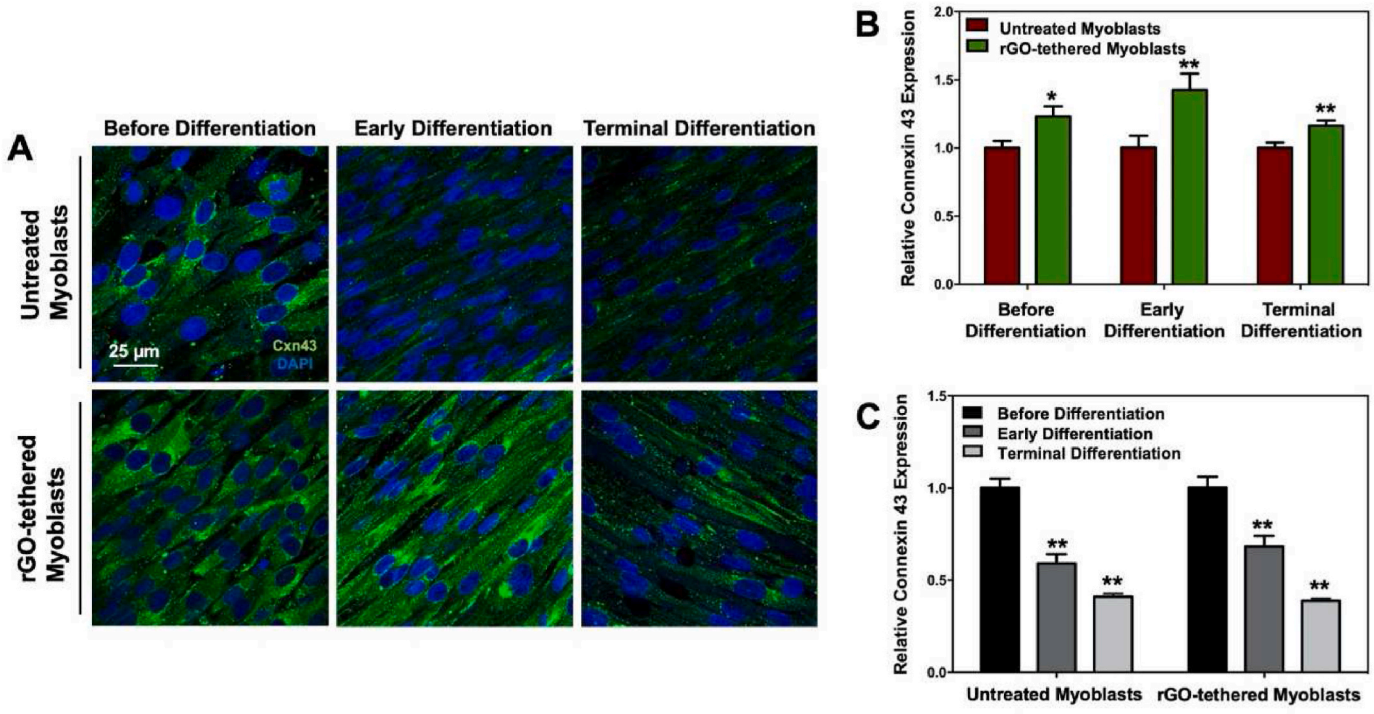

Fig. 2. Time-dependent change of the connexin 43 expression in skeletal myoblasts. (A) Immunofluorescence images of connexin 43 (Cxn 43, green) and nucleus (DAPI, blue) in untreated and rGO-tethered cells. (B) Relative connexin 43 expression level of rGO-tethered myoblasts normalized to untreated myoblasts before differentiation (day 3), at early differentiation (day 7), and at terminal differentiation (day 13). (C) Change in relative connexin 43 mRNA expression level in the untreated and rGO-tethered myoblasts over time. The values were normalized to those measured before differentiation (day 3) for each group. In (B) and (C), each bar value and error bar represent the average value and standard deviation of three different samples per condition (*$p < 0.05$, **$p < 0.01$). (For interpretation of the references to color in this figure legend, the reader is referred to the Web version of this article.)

PCR. Cells were evaluated at 3 different time points; before differentiation (day 3), early differentiation (day 7), and terminal differentiation (day 13). The immunofluorescence images of myosin heavy chain showed that untreated cells form MF20-positive myotubes during the early differentiation stage (Fig. 4A, first row). In contrast, rGO-tethered myoblasts developed MF20-positive myotubes before differentiation started (Fig. 3A, second row). The myoblasts were also stained with F-actin and sarcomeric α-actinin (Fig. 3B). Before differentiation, both untreated and rGO-tethered cells expressed F-actin only. As the differentiation proceeds, the multinucleated myotubes showed the sarcomeric α-actinins. Interestingly, the rGO-tethered cells formed larger myotubes with striated α-actinins than untreated cells.

These results illustrate that rGO flakes on myoblasts help to promote myogenic differentiation at the early stage. Given that rGO flakes serve to sustain cellular connexin 43 expressions at the early differentiation stage, the increased myogenic differentiation with rGO tethering is attributed to the extended duration of connexin 43. It is likely cells tethered by rGO flakes communicate better with adjacent cells through gap junctions, catalyzing the synthesis of myosin heavy chains [29].

The myogenic differentiation was also evaluated by examining myogenic gene expression using qRT-PCR (Fig. 4C). We compared mRNA expression levels of desmine (DES), myostatin (MSTN), myogenic factor 5 (MYF5), myogenic factor 5 (MYF5), myoblast determination protein (MYOD), myogenin (MYOG), troponin I (TNNI), and myosin heavy chain 1 (MHC1). These myogenic genes have been reported to regulate cell differentiation, myogenesis, and force generation [30,31]. Before initiation of differentiation (i.e., day 3), cells tethered with rGO flakes exhibited higher mRNA expressions for early myogenic proteins, including MYF5 (1.38 fold), MYOD (1.36 fold), and MYH1 (1.31 fold), than untreated cells. MYF5 and MYOD promote myogenic differentiation in an embryo, while MYH1 converts chemical energy to mechanical energy for muscle contraction. On day 7, rGO flakes on the cells increased MYOD (1.30 fold) and MYOG (1.37) gene expression levels. MYOG is another protein that promotes myogenic differentiation. The MYH1 gene expression was decreased slightly with rGO flakes, but no statistical significance of difference was found between conditions. On day 13, rGO flakes-tethered myoblasts showed a 1.24-fold increase in the MYF5 gene and a 1.47-fold increase in MYOD gene expressions, compared with untreated cells. In the previous section, we confirmed that rGO tethered to the myoblasts enhance connexin 43 expression level (Fig. 2). Altogether, we propose rGO promotes connexin 43 expression in myoblasts, which then supports cells to express myogenic markers after differentiation.

2.4. rGO flakes on the myoblasts regulate cellular genomics

We further examined the extent to which rGO regulates the whole genomic profile of myoblasts. Cells tethered with and without rGO were collected on day 3 (before differentiation) and day 13 (terminal differentiation stage) for analysis (Table 1). Before differentiation, untreated and rGO-tethered myoblasts expressed 160 different genes. At the terminal differentiation stage, the number of differentially expressed genes between two cell groups increased to 9452.

Based on the interaction result, we compared 7474 differentially

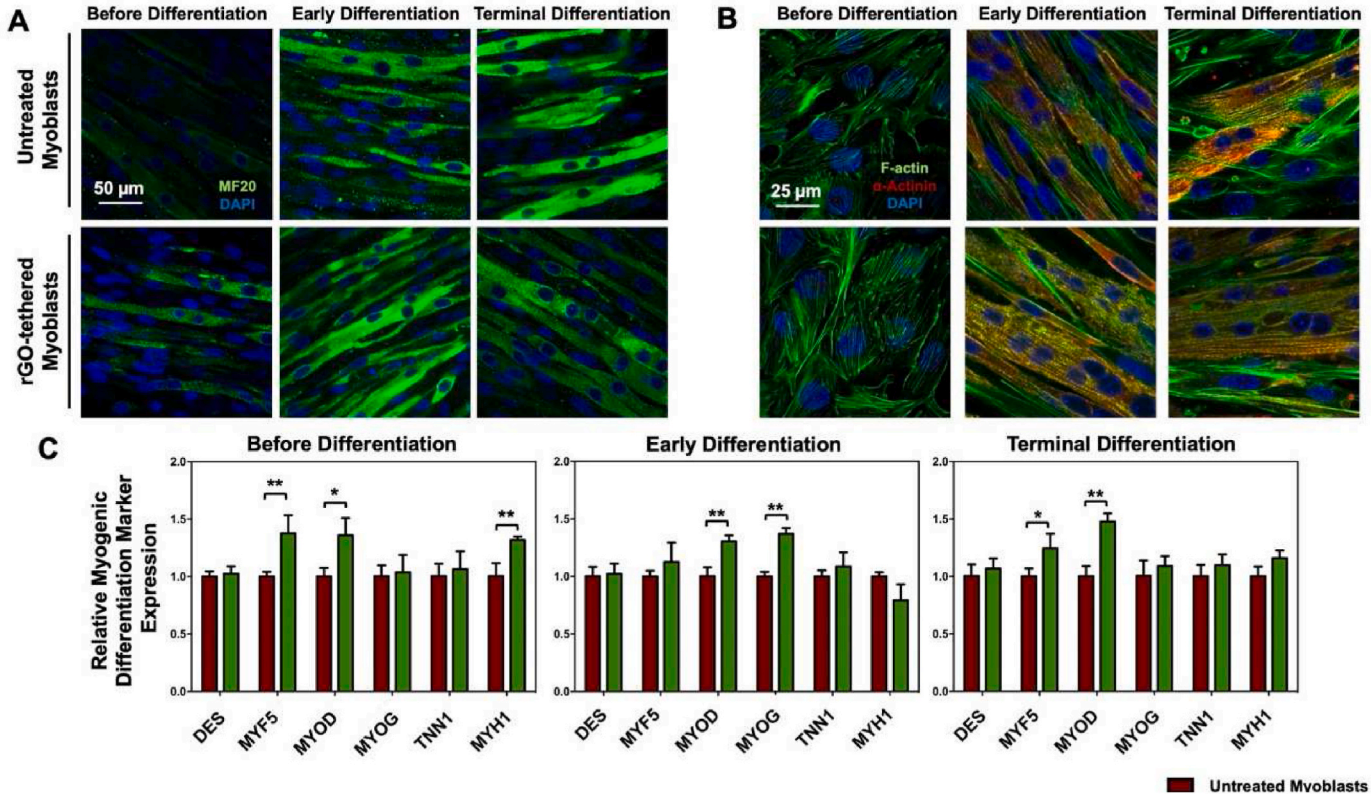

Fig. 3. Effects of rGO on myogenic differentiation (A) Immunofluorescently stained myotubes formed with untreated and rGO-tethered myoblasts. Myotubes were stained for myosin heavy chain (MF20, green) and nuclei (DAPI, blue). The images were captured before differentiation (day 3), at early differentiation (day 7), and at terminal differentiation (day 13). (B) Immunofluorescence images of myotubes stained for sarcomeric alpha-actinin (α-actinin, green) and nucleus (DAPI, blue). Both untreated and rGO-tethered cells were used to engineer myotubes. (C) Quantitative, real time-PCR analysis was performed to show relative myogenic marker gene expression levels in untreated and rGO-tethered myoblasts before differentiation (day 3), at early differentiation (day 7), and at terminal differentiation (day 13). The myogenic gene expression levels of rGO-tethered cells were normalized to that of untreated cells. Each bar value and error bar represent the average value and standard deviation of three different samples per condition (*$p < 0.05$, **$p < 0.01$). (For interpretation of the references to color in this figure legend, the reader is referred to the Web version of this article.)

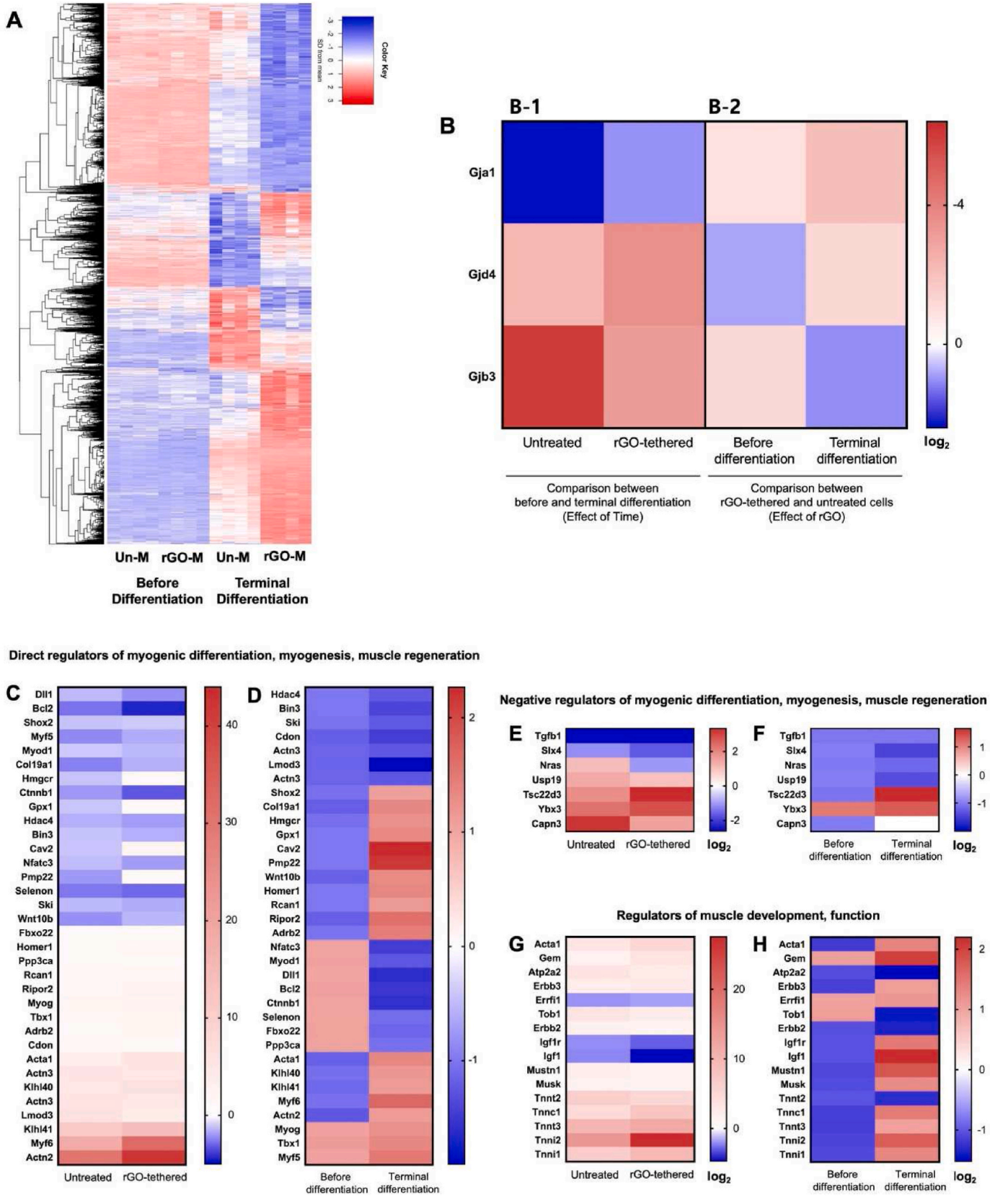

(caption on next page)

Fig. 4. rGO-induced gene expression profile analysis by RNA sequencing.(A) Heat map showing the differentially expressed genes (total 7474 genes, p-value<0.05, n = 4). The color key indicates the gene expression level; red indicates increased expression, and blue indicates decreased expression level. (B) Gap junction-related gene expression change in untreated and rGO-tethered myoblasts (FDR p-value<0.05). (C–F) Quantification of gene expression changes that regulate myogenesis, myogenic differentiation, and muscle regeneration. The genes were selected from the heat map. (C) displays the positive myogenic regulatory gene expression change between day 3 (before differentiation) and day 13 (terminal differentiation) for untreated and rGO-tethered cells. (D) displays the positive myogenic regulatory gene expression difference between rGO-tethered and untreated cells before differentiation and at the termination stage. (E) displays the negative myogenic regulatory gene expression change between day 3 (before differentiation) and day 13 (terminal differentiation) for untreated and rGO-tethered cells. (F) displays the negative myogenic regulatory gene expression difference between rGO-tethered and untreated cells before differentiation and at the termination stage. (G) displays the muscle development and function-related gene expression change between day 3 (before differentiation) and day 13 (terminal differentiation) for untreated and rGO-tethered cells. (H) displays the muscle development and function-related gene expression difference between rGO-tethered and untreated cells before differentiation and at the termination stage. For each graph, the order of the genes is based on the fold increase of the first column. . (For interpretation of the references to color in this figure legend, the reader is referred to the Web version of this article.)

Table 1
The number of differentially expressed genes analyzed with FDR p-value < 0.05. The effects of the rGO tethering and differentiation stage were separately analyzed to identify the number of upregulated and downregulated genes. Five contrasts were made to evaluate the effects of rGO, the effect of time, and lastly, the interaction (i.e., the time effect in the rGO group vs. the time effect in the control group).

	Effect of Time (Before Differentiation vs Terminal Differentiation)		Effect of rGO (Untreated Myoblasts vs rGO-tethered Myoblasts)		Interaction
	Untreated Myoblasts	rGO-tethered Myoblasts	Before Differentiation	Terminal Differentiation	
Down Regulated	5440	5887	132	4769	3734
Up Regulated	5393	5887	28	4683	3740
Not Significant	3197	2256	13,870	4578	N/A

expressed genes through differentiation with a $p < 0.05$ value and plotted those genes on a heatmap (Fig. 4A). The color key shows if the gene was relatively upregulated (red) or downregulated (blue). First, we tracked gap junction-related genes in the heatmap (Fig. 4B). Three genes include Gja1 (gap junction protein alpha 1) encoding connexin 43, Gjd4 (gap junction protein delta 4) encoding connexin 39, and Gjb3 (gap junction protein beta 3) encoding connexin 31. Both untreated and rGO-tethered myoblasts showed a decrease in Gja1 expression after differentiation. The downregulation, however, was less significant with rGO-tethered myoblasts. The expression of the Gjd4 gene was increased in cells tethered with rGO, implying the increased expression of connexin 39, which regulates embryonic muscle development and fusion [32,33]. The Gjb3 gene encoding connexin 31, not known to be expressed in skeletal muscle, was downregulated in rGO-tethered cells [34]. Separately, we compared the Gja1 gene expression of untreated cells with rGO-tethered cells (Fig. 4B). The rGO-tethered cells showed higher Gja1 gene expression levels than untreated cells at both pre-differentiation and terminal differentiation stages. The fold increase compared with untreated cells was more significant at the terminal differentiation stage.

We analyzed the genes regulating myogenic differentiation, myogenesis, and muscle regeneration (Fig. 4C and D). Untreated myoblasts exhibited up-regulation of 17 genes during differentiation. Interestingly, rGO tethered on the cells served to upregulate 11 genes, including Adrb2, Homer1, Rcan1, Ripor2, Tbx1, MyoG, Acta 1, Klhl40, Klhl41, Myf6, and Actn2 (Fig. 4C). In addition, 9 genes, including Ski, Selenon, Nfatc3, Bin3, Hdac4, Ctnnb1, Myod1, Bcl2, and Dll1, were down-regulated in the rGO-tethered myoblasts.

We additionally analyzed the effect of rGO on the myogenic gene expression patterns at pre-differentiation (day 3) and terminal differentiation stages (day 13) (Fig. 4D). Compared to the untreated cells, rGO-tethered myoblasts upregulated early myogenic markers, including Nfatc3, Myod1, Dll1, Bcl2, Ctnnb1, Selenon, Fbxo22, and Ppp3ca before differentiation [35,36]. These early markers were down-regulated at the terminal differentiation stage. The rGO-tethered myoblasts also down-regulated terminal differentiation markers including Klhl40, Khlh 41, Myf6, Actn2, Acta1 at day 3, and upregulated them at day 13 [37].

We further mapped the expression profiles of negative regulators for myogenic differentiation, myogenesis, and muscle regeneration. We first tracked the gene expression change throughout myogenic differentiation (Fig. 4E). Four out of seven negative regulators such as Slx4, Nras, Usp19, and Capn3 were down-regulated in rGO-tethered cells more significantly than untreated cells throughout differentiation (Fig. 4E). We also examined how rGO influenced negative gene expression before differentiation and at terminal differentiation. Five negative regulators, Tgfb1, Slx4, Nras, Usp19, and Capn3, were down-regulated at both time points (Fig. 4F).

In addition, we analyzed genes that involve muscle development and function (Fig. 4G and H). The rGO upregulated expressions of 4 genes encoding troponin subunits, troponin C, troponin T3, troponin I. Genes encoding actin and GTP-binding proteins were also upregulated during differentiation (Fig. 4G). Furthermore, genes encoding troponin T2, which plays a role in cardiac muscle contraction, were down-regulated in the rGO-tethered cells (Fig. 4H). rGO also stimulated cellular integrin and extracellular matrix protein (ECM)-related gene expressions. In particular, 20 out of 39 genes showed a greater increase over time with rGO tethered to the myoblasts (Supporting InformationFigure S3). Additionally, 10 out of 39 genes and 21 out of 39 genes showed an increase in presence of rGO at before differentiation and terminal differentiation stage, respectively (Supporting InformationFigure S3).

We further assessed the differentially expressed genes by performing gene ontology analysis (Supporting InformationTable S1 and S2). We first looked at the effect of time within the same group (Supporting InformationTable S1). The untreated myoblasts showed upregulation in various biological processes related to skeletal muscle differentiation, development, and function over time. The rGO-tethered myoblasts similarly showed an increase in various skeletal muscle-related biological processes. Additionally, they showed an increase in genes related to the musculoskeletal movement process and myofibril assembly compared with the untreated ones. Both groups showed an increase in the same cellular processes related to skeletal muscle development and neuromuscular junction formation. We also looked at which biological, cellular, and molecular functions were enhanced upon rGO treatment on days 3 and 10 (Supporting InformationTable S2).

Taken together, we suggest that these mRNA-Seq analyses disclose intracellular dynamic response to rGO on the cell surface during myogenic differentiation and myogenesis. During myogenic differentiation, multiple signaling pathways change in response to fusion and development [38–40]. The rGO flakes did not alter gene expression patterns dramatically at the early differentiation stage but made significant changes at the terminal differentiation stage. This result may be attributed to the increase in the retention of ECM proteins on the cell surface. We have observed that tethering rGO to the myoblasts increased the number of extracellular matrix-related gene expression levels greater in the terminal differentiation stage (Supporting

InformationFigure S3). Based on our result, it may be concluded that the presence of rGO enhances the expression of these proteins and thus, facilitates the interaction between the cells and ECM.

2.5. Enhanced pump-bot performance by rGO-tethered myoblasts

Our results above confirmed that rGO flakes on the cells serve to upregulate connexin 43 and myogenic factor-encoding gene expressions. This section sought if the gap junction proteins and subsequent genetic changes improve the contraction of rGO-tethered myotubes. For this analysis, we utilized a valveless, biohybrid pumping machine called "pump-bot" that can generate unidirectional fluid flow powered by engineered skeletal muscle [6,41].

Inspired by an embryonic vertebrate heart, a contractile muscle ring surrounds an off-center part of a resilient and durable hydrogel tube which is connected to a stiffer silicone tube (Supporting InformationFigure S4). Continued muscle contractions along the circumferential direction compress the gel tube in the radial direction and drive a unidirectional fluid flow due to elastic waves propagating along the gel tube and bouncing pack at the gel/silicone tube connection. Therefore, this pump-bot is helpful to evaluate the contractility of engineered muscle.

We engineered a 5 mm-diameter 3D muscle ring with myoblasts tethered with rGO. The rGO-tethered muscle rings are colored in black, confirming the presence of rGOs on myoblasts (Fig. 5A, muscle ring in black dashed box). The muscle ring fabricated with rGO-free myoblasts was white (Fig. 5A, muscle ring in red box). We placed the muscle ring on a flexible 4-mm diameter polyacrylamide hydrogel tube. The tube was assembled into a closed microfluidic system fabricated with polydimethylsiloxane (PDMS) (Fig. 5A).

We first measured the cyclic tube deformation caused by the electrical stimulation of muscle (9 V pulse with 10 ms pulse width) (Fig. 5B). According to the image, the average tube wall displacement at the diametric plane was around 27 μm, according to the image processing. The rGO-tethered muscle exhibited the same contraction frequency as the untreated muscle. However, the rGO-tethered muscle led to the 3-fold increase of the average wall displacement to 73 μm.

We examined the fluid flow created by muscle contraction and subsequent gel tube deformation. We tracked trajectories of fluorescent beads in three different radial positions of the gel tube (Fig. 5C). The average fluid velocity at the different radial positions was calculated with the linear fitting. The mean flow profile over the cross-section was parabolic (Fig. 5D). The maximum average velocity at the center of the gel tube was 27.47 μm/s with the untreated muscle ring (Fig. 5E). Notably, the rGO-tethered muscle ring made a 2.2-fold increase of the maximum average velocity to 59.8 μm/s. The increase in the fluid velocity is comparable to the tube displacement increase, indicating that fluid flow depends on the muscle contraction force, not frequency.

Accordingly, the flow rate (Q) = $\pi r^2 V$, where the r is the tube radius, and V is the average fluid velocity along the tube cross-section, was increased from 14.42 to 28.83 μl/min with the use of rGO-tethered muscle ring (Fig. 5F). In addition, the Reynolds number (Re) = $\rho Vd/\eta$, where ρ is the fluid density, d is the inner tube diameter, and η is the dynamic viscosity of culture medium at 37 °C (0.82 cP), was increased

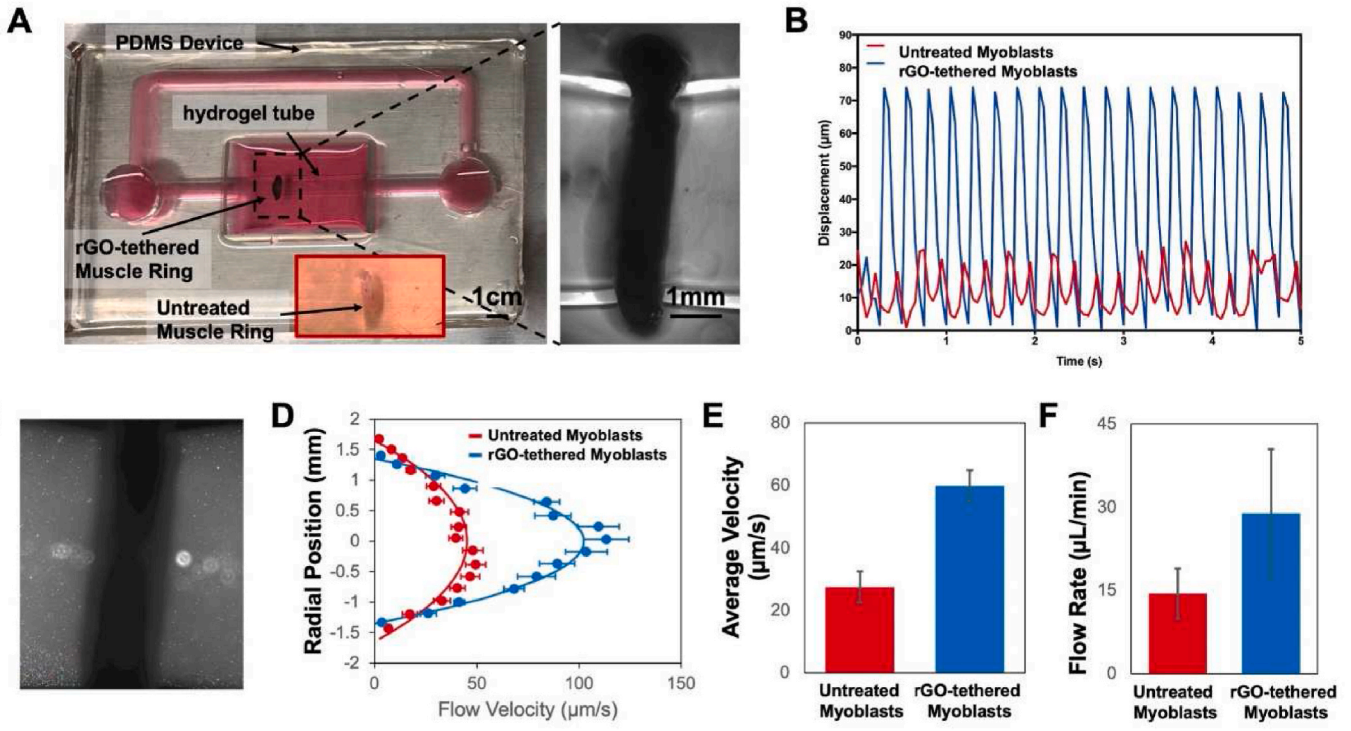

Fig. 5. Effects of the rGO-tethered muscle ring on the performance of biohybrid pump named pump-bot (A) Image of the pump-bot assembled using the rGO-tethered muscle ring. The skeletal muscle ring prepared with untethered myoblasts is shown in the red box. The pump-bot consists of a flexible polyacrylamide gel tube connected to a rigid silicone tube. The engineered skeletal muscle ring wraps around the gel tube at an off-center position. The electrical stimulation causes circumferential muscle contraction, and subsequent tube compression in the radial direction drives a unidirectional fluid flow. The enlarged image shows the phase contrast image of the skeletal muscle ring around the flexible gel tube. (B) Representative deformation graph of the hydrogel tube. (C) Representative fluorescence image used to detect the fluid flow in the pump-bot. The fluorescence beads were detected using ImageJ software. (D) Flow velocity profiles of representative samples from untreated myoblasts and rGO-tethered myoblasts groups. Velocity values are mean ± SE with n = 12 measurements at each radial position. Overlaid curves are parabolic fits to mean values. (E) Average flow velocity: values are mean ± SD with n = 3 experiments each for untreated and rGO-tethered myoblasts groups. rGO-tethered muscle rings provide 2.2-fold higher flow velocity (p value = 0.07). (F) Flow rate: values are mean ± SD with n = 3 experiments each for untreated and rGO-tethered groups. rGO-tethered muscle rings provide a 2-fold higher flow rate (p value = 0.18). (For interpretation of the references to color in this figure legend, the reader is referred to the Web version of this article.)

from 0.27 to 0.58.

Coupled with the whole RNA sequencing analysis shown in Fig. 4, we propose that muscle contraction increased by rGO tethering is due to up-regulation of troponin. The troponin acts as a control switch that senses the cytosolic calcium increase and makes the striated muscle contract and produces force [42,43]. The protein consists of 3 subunits, troponin C, troponin I, and troponin T. We found that rGO tethered to myoblasts increased levels of genes encoding troponin I, troponin T3, and troponin C. Therefore, it is highly likely that troponins led to active muscle contraction and, in turn, enhanced pump-bot performance.

2.6. Enhanced light-triggered contraction of rGO-tethered myotubes

We further tested if rGO tethered to myoblasts increases the muscle contraction force in response to electrical and optical stimulus (Fig. 6). We used Channel rhodopsin transfected myoblasts, which express light-sensitive ion channels. The myotubes formed with the engineered cells contract in response to 470 nm blue LED light [31,44]. For this analysis, we cultured the untreated myoblasts and rGO-tethered myoblasts on a glass-bottom dish and plotted the displacement of cells in both the x and y-axis (Fig. 6A). The electric field applied with two-wire electrodes or the optimal stimulus made with LED triggered the displacement of the myotubes for both untreated myoblasts and rGO-tethered myoblasts (Fig. 6B).

Specifically, rGO on myoblasts increased the electrically or optically triggered muscle displacement by 1.5 times compared with untreated myoblasts. The magnitude of contraction increase was also 1.4-fold higher with rGO-tethered myoblasts. These results suggest that the mechanism by which rGO improves muscle contraction hinges on extended connexin 43 expression and increased myotube maturation. Thus, we proposed that the electrical conductivity of rGO is a minor factor because both electrical and optical stimulation increase rGO-tethered muscle contraction with a similar fold change.

3. Conclusion

In conclusion, this study demonstrates that extending the duration of connexin 43 on skeletal myoblasts significantly enhances the quality of muscle engineered in vitro. Tethering rGO flakes onto myoblasts circumvented early down-regulation of connexin 43 during myogenic differentiation. As a result, rGO enhanced myogenic differentiation, confirmed with the immunostaining, RT-PCR, and whole-genome profile analysis. The rGO-tethered myotubes also generated a three-fold larger contraction in a biohybrid pump than rGO-free myotubes, increasing both fluid velocity and flow rate. Combined with the genomic analysis, we suggest that the enhanced muscle contraction is related to the increased troponin synthesis in the myotubes. We also propose that the rGO-tethered skeletal muscle tissue has the potential to repair injured or defective skeletal muscle, which will be examined systematically in future studies. Overall, this study provides a foundation for improving the physiological activities of engineered muscle and further the performance of the biological machine. This study will significantly impact methods to recreate tissue and organoid platforms for fundamental and applied bioscience studies on development, disease, and new therapeutics.

4. Materials and methods

4.1. Characterization and analysis of rGO

The rGO flakes were purchased from ACS Materials (ACS Material LLC, CA). The rGO flakes were characterized by the Raman spectroscopy (Raman-11, Nanophoton) that uses argon laser operating at 514 nm as an excitation source. The morphology of rGO flakes was analyzed with images captured using transmission electron microscopy (TEM, JEOL 2100 TEM). The length and width of an individual rGO flake were measured using ImageJ.

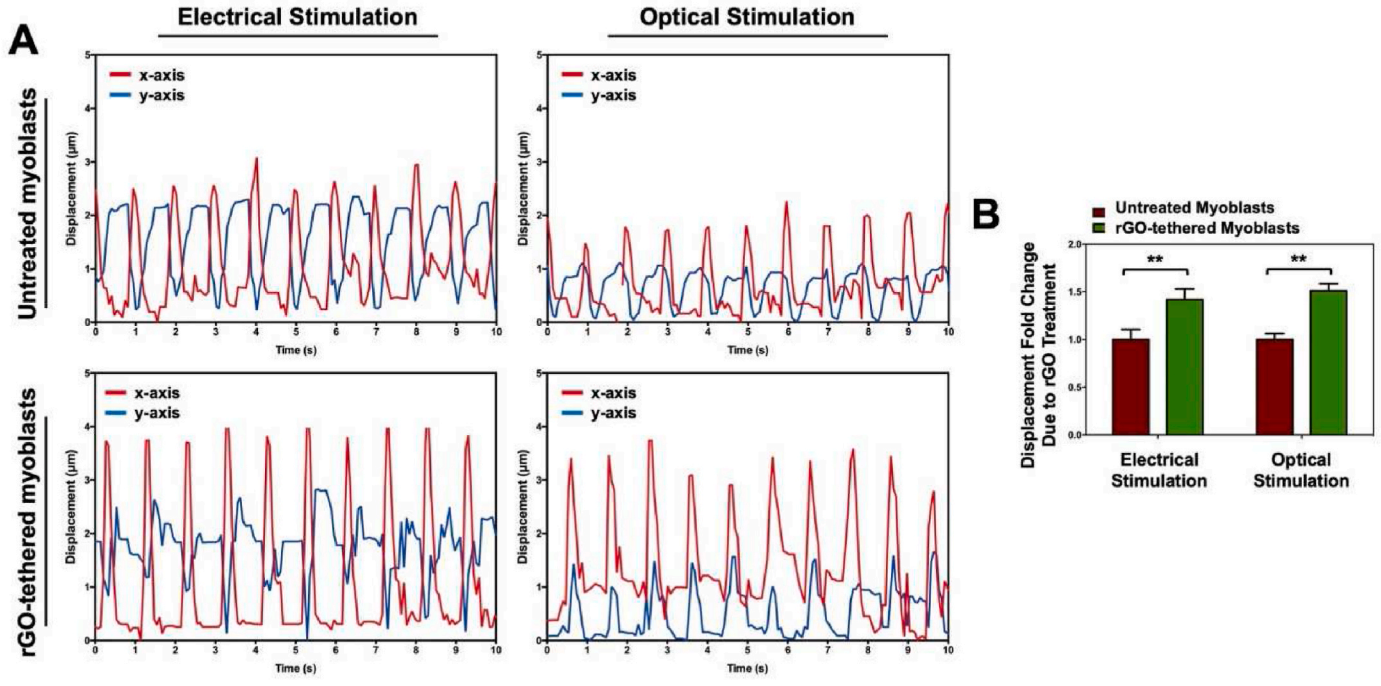

Fig. 6. Response of a muscle sheet to electrical or optical stimulation. Skeletal myoblasts were engineered to express channelrhodopsin to examine if rGO tethered to cells enhances muscle contraction in response to electrical current or LED light. (A) The displacement of myotubes through the x-axis and y-axis was recorded and plotted on a displacement vs. time graph. (B) The relative fold change in displacement in the presence of rGO upon electrical and optical stimulations was plotted. (n = 8, * and ** represent the statistical significance between the values. *$p < 0.01$, **$p < 0.05$).

4.2. C2C12 skeletal myoblast culture

Cells plated on a 2D substrate were cultured in a growth medium consisting of Dulbecco's modified Eagle medium (DMEM) (Corning Cellgro) supplemented with 10% (vol/vol) fetal bovine serum (FBS, Lonza), 1% (vol/vol) L-glutamine (Cellgro Mediatech), and 1% (vol/vol) penicillin-streptomycin (PS, Gibco). For myogenic differentiation, the growth medium was replaced with a differentiation medium (DMEM supplemented with 10% horse serum, 1% PS, 1% L-glutamine and IGF-1) after day 3 in the growth medium. The cells were incubated in the differentiation medium for additional 11 days. Both growth and differentiation medium were supplemented with the fibrinolytic inhibitor aminocaproic acid (ACA, 1 mg/ml).

4.3. Tethering rGO to cells

The stock of 5 mg/ml rGO suspended in ethanol was prepared. The stock suspension was pipetted well and sterilized under UV for 30 min. Then, the stock suspension was vortexed at maximum speed for 10 min and sonicated in a bath sonicator for an additional 30 min. The stock solution was diluted in the growth medium at a concentration of 5 μg/ml. The myoblasts, which reached 80% confluency, were incubated with rGO overnight at 37 °C. The next day, cells tethered with rGO were collected by trypsinizing the cells from the cell culture flask. The cells were centrifuged to remove excess rGO for further use.

4.4. Analysis of rGO tethered on cells

rGO tethered on the cell was visualized by quenching effect [45]. Cells tethered with rGO were plated on a glass-bottom dish with a growth medium and were covered with a layer of fluorescent dye by spin coating. The coating solution was prepared by adding 1 mg of fluorescein sodium salt powder in 10 ml of 0.5 wt % polyvinylpyrrolidone (PVP, Sigma-Aldrich, Mw = 360,000)/ethanol solution. 100 μl of the coating solution was dispensed on the glass area and spun for 5 s at 500 rpm and 45 s at 4000 rpm. The quenched area was visualized by the decrease in the quantum yield of fluorescence induced by the molecular interaction with rGO while exciting the fluorescein by 488 nm laser beam under Zeiss LSM 700.

4.5. Cytotoxicity test

Trypan blue exclusion assay was used to determine the number of viable cells after the rGO tethering. Myoblasts were incubated with 0 μg/ml, 3 μg/ml, 5 μg/ml, and 10 μg/ml of rGO flakes in the growth medium. After 24 h, the media was changed to growth media without rGO. The cells were collected on days 1, 3, 7, and 10. Then, the viable cells were counted after treating with trypan blue solution. Nine sections on the hemacytometer were counted, and a total of 4 samples were analyzed per condition each day to verify the result. We also examined the viability of the myoblasts using the LIVE/DEAD™ Viability/Cytotoxicity Kit (Invitrogen, Carlsbad, CA). The C2C12 myoblasts were mixed with rGO suspended media at 0 μg/ml, 3 μg/ml, 5 μg/ml, and 10 μg/ml and incubated for 24 h. Then, the media was changed to growth media without rGO. The cells were stained according to the manufacturer's protocol, and the nuclei were additionally stained with Hoechst 33,342 (5 μg/mL, 30 min). We counted the total number of cells and subtracted the number of dead cells to quantify the cell viability.

4.6. Immunocytochemical analysis

Differentiated cells were analyzed with immunostaining for connexin 43 and myotubes. Cells were fixed in 4% (w/v) paraformaldehyde (Sigma) for 30 min, permeablized with 0.1% (v/v) Triton X-100 (Sigma) for 5 min and incubated in a 2% goat serum for 45 min at room temperature. After completing each step, the samples were washed with PBS 2 times. After blocking, cells were incubated with primary antibodies at 4 °C overnight. To stain for connexin 43, cells were incubated with anti-connexin43 (GJA1 antibody, Abcam, Cambridge, U.K.). To stain for myogenic markers, another set of cells were incubated in a solution of MF-20 anti-MHC (1:400) (iT FX, Developmental Studies Hybridoma Bank, The University of Iowa Department of Biology) or a solution of anti-sarcomeric α-actinin antibody (Abcam, Cambridge, U.K.). On the next day, cells were washed with PBS twice. Then, anti-connexin43 was labeled with Alexa Fluor-488 donkey anti-rabbit IgG (1:500; Invitrogen). Cells incubated with MF-20 were treated with Alexa Fluor-488 goat anti-mouse IgG (1:500; Invitrogen), and those incubated with anti-sarcomeric α-actinin antibody were treated with Alexa Fluor-568 donkey anti-rabbit IgG (1:500) (Invitrogen) and fluorescein (FITC)-conjugated Phalloidin. All samples were incubated with secondary antibodies for 1 h. Finally, the nuclei were labeled with 4′,6-Diamidino-2-Phenylindole (DAPI, Sigma). The fluorescence images were obtained with a multiphoton confocal microscope (LSM 710, Carl Zeiss).

4.7. Quantitative real-time polymerase chain reaction analysis

Quantitative real-time polymerase chain reaction (qRT-PCR) analysis was conducted at 3 different time points; before differentiation (day 3 after seeding), early differentiation (day 7 after seeding), and terminal differentiation (day 10 after seeding). Note that the growth medium was replaced with the differentiation medium on day 3. Total RNA from the samples was extracted from cells using the RNeasy Mini Kit (Qiagen) following the manufacturer's protocol. After extracting the mRNA, cDNA synthesis was performed with qScript cDNA Super Mix (Quanta Biosciences) from 100 ng of RNA, and the reaction was performed according to the manufacturer's protocol. Then, SsoFast EvaGreen Supermix (Bio-Rad) was added to the cDNA and primers, and the mixtures were analyzed using CFX Connect Real-Time System (Bio-Rad). For the analysis, the cycle threshold (Ct) values were compared relative to the GAPDH and control samples. All primer sequences used for the qRT-PCR analysis have been reported in Supporting Information. Table S3.

4.8. RNA sequencing analysis

The RNA samples were prepared with TruSeq Stranded mRNA-seq Sample Prep kits(Illumina). Differential gene expression analysis was performed using the limma-trend method on the logCPM values. Total 5 comparisons were made; (1) Before differentiation vs. Terminal differentiation of the untreated cells, (2) before differentiation vs. terminal differentiation of the rGO-tethered cells, (3) rGO-tethered cells vs. untreated cells before differentiation stage, (4) rGO-tethered cells vs. untreated cells at terminal differentiation stage, and (5) time effect for the rGO-tethered cells vs. time effect for the untreated cells. Multiple testing correction was done separately for each comparison using the False Discovery Rate (FDR) method. The differential expression was considered significant at FDR p-value < 0.05. Gene ontology enrichment analysis was performed by assessing the list of differentially expressed genes on the gene ontology database (http://www.geneontology.org).

4.9. Engineering of 3D myoblasts ring

Cells tethered with rGO or untreated cells were suspended at a concentration of 1.0×10^7 cells/ml in a mixture composed of growth medium supplemented with 30% v/v Matrigel (BD Biosciences), 4 mg/ml fibrinogen (Sigma), 0.5 U/mg thrombin (Sigma). Each well in the PDMS ring mold was filled with 150 μl cell mixture and incubated at 37 °C for 1 h. After the cell-gel mixture compacted, muscle rings were immersed in a growth medium.

4.10. Hydrogel tube preparation for pump-bot assembly

1 ml of 40% w/v aqueous solution of acrylamide, 4 μl of 2% w/v

methylene bis-acrylamide, 10 μl of 10% w/v ammonium persulfate, and 2 μl of tetramethylene diamine was mixed together [46]. The mixture was loaded into a 3D printed hollow mold and left at room temperature for 30 min. Then, the mold was removed to retrieve the hydrogel tube. The gel tube was incubated in water overnight. The outer diameter and inner diameter of the hydrogel tubes are 4 and 3 mm, respectively.

4.11. Pump-bot assembly and analysis

The muscle ring was placed on the fabricated hydrogel tube after being incubated in a growth medium for 2 days (Supporting InformationFigure S5). After the muscle ring was placed on the tube, the ring was incubated for another day in the growth medium. On day 3 after the muscle ring was formed, the growth medium was exchanged with the differentiation medium. The muscle-gel tube pair was incubated in the differentiation medium for another 7 days. Finally, the muscle-tube complex was placed on the Pump-bot platform by connecting two ends of the gel tube with the PDMS channel. After assembling the Pump-bot, FITC-tagged polystyrene beads (diameter = 1 μm, BD Bioscience) were dispersed into the media that flows through the hydrogel tube. The movement of fluorescent beads was captured with the Olympus IX81 inverted microscope (Olympus). While imaging, the samples were maintained with 37 °C and 5% CO_2 in an environmental chamber. To stimulate muscle contraction, we applied bipolar electrical pulses (9 V, 10 ms pulse width) by placing two wire electrodes were placed either side of the muscle ring. The information on the recorded movies is written down on Supporting Information. Table S4.

4.12. Analysis of rGO conductivity

We transfected the Channelrhodopsin gene into the skeletal myoblasts. After confirming cells express the channelrhodopsin, the cells were tethered with rGO overnight and plated on a tissue culture plate. After the cells were cultured in a growth medium for 3 days and a differentiation medium for 10 days, the cells were stimulated both optically and electrically. The muscle layer was optically stimulated with a 470 nm LED (Mightex Systems Inc) with 50 ms pulses of 1 Hz frequency. Separately, the muscle layer was stimulated electrically with a custom-built electrical stimulation unit. The biphasic electrical pulses of 20 V amplitude and 50 ms pulse width were applied to the muscle layer. All videos were recorded with Olympus ix81 inverted microscope (Olympus) and used to measure the displacement of the muscle layer. The information on the recorded movies is written down on Supporting InformationTable S4.

4.13. Statistical analysis

The statistical analyses were performed using unpaired Student's t-test with Graph Pad Prism 6.0 (Graph Pad Software Inc., San Diego, CA, USA). Statistical differences were considered significant at a p-value smaller than 0.05.

Author contribution

Eunkyung Ko: Conceptualization, methodology, writing-original draft. **Onur Aydin**: Software, formal analysis, writing - Review & Editing. **Zhengwei Li**: Software, formal analysis, writing - Review & Editing. **Lauren Gapinske**: Investigation, writing - Review & Editing. **Kai-Yu Huang**: Investigation, writing - Review & Editing. **Taher Saif**: Resources, writing - Review & Editing. **Rashid Bashir**: writing - Review & Editing, Supervision. **Hyunjoon Kong**: writing - Review & Editing, Supervision.

Declaration of competing interest

The authors declare that they have no known competing financial interests or personal relationships that could have appeared to influence the work reported in this paper.

Acknowledgements

This work was supported by the National Science Foundation (CBET-1932192 & STC-EBICS Grant CBET-0939511), the National Institute of Biomedical Imaging and Bioengineering of the National Institutes of Health (T32EB019944 to E. Ko), and the Korean Institute of Science and Technology-Europe. The content is solely the authors' responsibility and does not necessarily represent the official views of the National Institutes of Health. We want to thank Dr. Alvaro G. Hernández, Dr. Chris L. Wright, and Dr. Christopher J. Fields from the Roy J. Carver Biotechnology Center for the help in producing RNA Sequencing libraries.

Appendix A. Supplementary data

Supplementary data to this article can be found online at https://doi.org/10.1016/j.biomaterials.2022.121643.

References

[1] S. Carosio, L. Barberi, E. Rizzuto, C. Nicoletti, Z. Del Prete, A. Musaro, Generation of ex vivo-vascularized muscle engineered tissue (X-MET), Sci. Rep. 3 (1) (2013) 1–9.
[2] J.H. Kim, Y.-J. Seol, I.K. Ko, H.-W. Kang, Y.K. Lee, J.J. Yoo, A. Atala, S.J. Lee, 3D bioprinted human skeletal muscle constructs for muscle function restoration, Sci. Rep. 8 (1) (2018) 1–15.
[3] L. Grant, R. Raman, C. Cvetkovic, M.C. Ferrall-Fairbanks, G.J. Pagan-Diaz, P. Hadley, E. Ko, M.O. Platt, R. Bashir, Long-term cryopreservation and revival of tissue-engineered skeletal muscle, Tissue Eng. 25 (13–14) (2019) 1023–1036.
[4] C. Cvetkovic, M.C. Ferrall-Fairbanks, E. Ko, L. Grant, H. Kong, M.O. Platt, R. Bashir, Investigating the life expectancy and proteolytic degradation of engineered skeletal muscle biological machines, Sci. Rep. 7 (1) (2017) 1–13.
[5] G.J. Pagan-Diaz, X. Zhang, L. Grant, Y. Kim, O. Aydin, C. Cvetkovic, E. Ko, E. Solomon, J. Hollis, H. Kong, Simulation and fabrication of stronger, larger, and faster walking biohybrid machines, Adv. Funct. Mater. 28 (23) (2018), 1801145.
[6] Z. Li, Y. Seo, O. Aydin, M. Elhebeary, R.D. Kamm, H. Kong, M.T.A. Saif, Biohybrid valveless pump-bot powered by engineered skeletal muscle, Proc. Natl. Acad. Sci. USA 116 (5) (2019) 1543–1548.
[7] H. Kim, M.-C. Kim, H.H. Asada, Extracellular matrix remodelling induced by alternating electrical and mechanical stimulations increases the contraction of engineered skeletal muscle tissues, Sci. Rep. 9 (1) (2019) 1–11.
[8] B.C. Syverud, K.W. VanDusen, L.M. Larkin, Growth factors for skeletal muscle tissue engineering, Cells Tissues Organs 202 (3–4) (2016) 169–179.
[9] B.C. Anderson, S.P. Christiansen, S. Grandt, R.W. Grange, L.K. McLoon, Increased extraocular muscle strength with direct injection of insulin-like growth factor-I, Investig. Ophthalmol. Vis. Sci. 47 (6) (2006) 2461–2467.
[10] G. Meşe, G. Richard, T.W. White, Gap junctions: basic structure and function, J. Invest. Dermatol. 127 (11) (2007) 2516–2524.
[11] N.M. Kumar, N.B. Gilula, The gap junction communication channel, Cell 84 (3) (1996) 381–388.
[12] F.E. LeBeau, R.D. Traub, H. Monyer, M.A. Whittington, E.H. Buhl, The role of electrical signaling via gap junctions in the generation of fast network oscillations, Brain Res. Bull. 62 (1) (2003) 3–13.
[13] J.-C. Hervé, M. Derangeon, Gap-junction-mediated cell-to-cell communication, Cell Tissue Res. 352 (1) (2013) 21–31.
[14] D.B. Alexander, G.S. Goldberg, Transfer of biologically important molecules between cells through gap junction channels, Curr. Med. Chem. 10 (19) (2003) 2045–2058.
[15] H.M. van der Velden, H.J. Jongsma, Cardiac gap junctions and connexins: their role in atrial fibrillation and potential as therapeutic targets, Cardiovasc. Res. 54 (2) (2002) 270–279.
[16] P.A. Merrifield, D.W. Laird, Connexins in Skeletal Muscle Development and Disease, Seminars in Cell & Developmental Biology, Elsevier, 2016, pp. 67–73.
[17] R. Araya, D. Eckardt, M.A. Riquelme, K. Willecke, J.C. Sáez, Presence and importance of connexin43 during myogenesis, Cell Commun. Adhes. 10 (4–6) (2003) 451–456.
[18] A. Proulx, P.A. Merrifield, C.C. Naus, Blocking gap junctional intercellular communication in myoblasts inhibits myogenin and MRF4 expression, Dev. Genet. 20 (2) (1997) 133–144.
[19] H. Shen, S. Grimston, R. Civitelli, S. Thomopoulos, Deletion of connexin43 in osteoblasts/osteocytes leads to impaired muscle formation in mice, J. Bone Miner. Res. 30 (4) (2015) 596–605.
[20] J.-T. Jeong, M.-K. Choi, Y. Sim, J.-T. Lim, G.-S. Kim, M.-J. Seong, J.-H. Hyung, K. S. Kim, A. Umar, S.-K. Lee, Effect of graphene oxide ratio on the cell adhesion and growth behavior on a graphene oxide-coated silicon substrate, Sci. Rep. 6 (1) (2016) 1–10.

[21] A. Aryaei, A.H. Jayatissa, A.C. Jayasuriya, The effect of graphene substrate on osteoblast cell adhesion and proliferation, J. Biomed. Mater. Res. 102 (9) (2014) 3282–3290.
[22] Y.C. Shin, J.H. Lee, L. Jin, M.J. Kim, Y.-J. Kim, J.K. Hyun, T.-G. Jung, S.W. Hong, D.-W. Han, Stimulated myoblast differentiation on graphene oxide-impregnated PLGA-collagen hybrid fibre matrices, J. Nanobiotechnol. 13 (1) (2015) 1–11.
[23] J. Aparicio-Collado, N. García-San-Martín, J. Molina-Mateo, C.T. Cabanilles, V. D. Quiles, A. Serrano-Aroca, R.S. i Serra, Electroactive calcium-alginate/polycaprolactone/reduced graphene oxide nanohybrid hydrogels for skeletal muscle tissue engineering, Colloids Surf. B Biointerfaces 214 (2022), 112455.
[24] X. Zhao, Z. Zhang, J. Luo, Z. Wu, Z. Yang, S. Zhou, Y. Tu, Y. Huang, Y. Han, B. Guo, Biomimetic, highly elastic conductive and hemostatic gelatin/rGO-based nanocomposite cryogel to improve 3D myogenic differentiation and guide in vivo skeletal muscle regeneration, Appl. Mater. Today 26 (2022), 101365.
[25] J. Von Maltzahn, V. Wulf, K. Willecke, Spatiotemporal expression of connexin 39 and− 43 during myoblast differentiation in cultured cells and in the mouse embryo, Cell Commun. Adhes. 13 (1–2) (2006) 55–60.
[26] L. Rueda-Gensini, J.A. Serna, J. Cifuentes, J.C. Cruz, C. Muñoz-Camargo, Graphene oxide-embedded extracellular matrix-derived hydrogel as a multiresponsive platform for 3D bioprinting applications, Int. J. Bioprinting 7 (3) (2021).
[27] J. Park, Y.S. Kim, S. Ryu, W.S. Kang, S. Park, J. Han, H.C. Jeong, B.H. Hong, Y. Ahn, B.S. Kim, Graphene potentiates the myocardial repair efficacy of mesenchymal stem cells by stimulating the expression of angiogenic growth factors and gap junction protein, Adv. Funct. Mater. 25 (17) (2015) 2590–2600.
[28] I. ISO, 10993–5: 2009 Biological Evaluation of Medical Devices—Part 5: Tests for in Vitro Cytotoxicity, International Organization for Standardization, Geneva, 2009.
[29] K. Suzuki, N.J. Brand, S. Allen, M.A. Khan, A.O. Farrell, B. Murtuza, R.E. Oakley, M.H. Yacoub, Overexpression of connexin43 in skeletal myoblasts: relevance to cell transplantation to the heart, J. Thorac. Cardiovasc. Surg. 122 (2001) 759–766.
[30] P. Heher, B. Maleiner, J. Prüller, A.H. Teuschl, J. Kollmitzer, X. Monforte, S. Wolbank, H. Redl, D. Rünzler, C. Fuchs, A novel bioreactor for the generation of highly aligned 3D skeletal muscle-like constructs through orientation of fibrin via application of static strain, Acta Biomater. 24 (2015) 251–265.
[31] R. Raman, L. Grant, Y. Seo, C. Cvetkovic, M. Gapinske, A. Palasz, H. Dabbous, H. Kong, P.P. Pinera, R. Bashir, Damage, healing, and remodeling in optogenetic skeletal muscle bioactuators, Adv. Healthc. Mater. 6 (12) (2017), 1700030.
[32] R. Araya, D. Eckardt, S. Maxeiner, O. Krüger, M. Theis, K. Willecke, J.C. Sáez, Expression of connexins during differentiation and regeneration of skeletal muscle: functional relevance of connexin43, J. Cell Sci. 118 (1) (2005) 27–37.
[33] A. Trovato-Salinaro, N. Belluardo, M. Frinchi, J. von Maltzahn, K. Willecke, D. F. Condorelli, G. Mudo, Regulation of connexin gene expression during skeletal muscle regeneration in the adult rat, Am. J. Physiol. Cell Physiol. 296 (3) (2009) C593–C606.
[34] B.W. Mok, W.S. Yeung, J.M. Luk, Differential expression of gap-junction gene connexin 31 in seminiferous epithelium of rat testes, FEBS Lett. 453 (3) (1999) 243–248.
[35] U. Delling, J. Tureckova, H.W. Lim, L.J. De Windt, P. Rotwein, J.D. Molkentin, A calcineurin-NFATc3-dependent pathway regulates skeletal muscle differentiation and slow myosin heavy-chain expression, Mol. Cell Biol. 20 (17) (2000) 6600–6611.
[36] Y. Zhang, I. Lahmann, K. Baum, H. Shimojo, P. Mourikis, J. Wolf, R. Kageyama, C. Birchmeier, Oscillations of Delta-like1 regulate the balance between differentiation and maintenance of muscle stem cells, Nat. Commun. 12 (1) (2021) 1–16.
[37] C.A. Goodman, J.R. Davey, A. Hagg, B.L. Parker, P. Gregorevic, Dynamic changes to the skeletal muscle proteome and ubiquitinome induced by the E3 ligase, ASB2β, Mol. Cell. Proteomics 20 (2021).
[38] S.M. Hindi, M.M. Tajrishi, A. Kumar, Signaling mechanisms in mammalian myoblast fusion, Sci. Signal. 6 (272) (2013) re2-re2.
[39] J. Chal, O. Pourquié, Making muscle: skeletal myogenesis in vivo and in vitro, Development 144 (12) (2017) 2104–2122.
[40] A. Blais, M. Tsikitis, D. Acosta-Alvear, R. Sharan, Y. Kluger, B.D. Dynlacht, An initial blueprint for myogenic differentiation, Genes Dev. 19 (5) (2005) 553–569.
[41] Z. Li, W. Ballance, M. Joy, S. Patel, J. Hwang, H. Kong, T.A. Saif, Adaptive biohybrid pumping machine with flow loop feedback, Biofabrication 14 (2022).
[42] A.V. Gomes, J.D. Potter, D. Szczesna-Cordary, The role of troponins in muscle contraction, IUBMB Life 54 (6) (2002) 323–333.
[43] Z. Yang, M. Yamazaki, Q.W. Shen, D.R. Swartz, Differences between cardiac and skeletal troponin interaction with the thin filament probed by troponin exchange in skeletal myofibrils, Biophys. J. 97 (1) (2009) 183–194.
[44] R. Raman, C. Cvetkovic, S.G. Uzel, R.J. Platt, P. Sengupta, R.D. Kamm, R. Bashir, Optogenetic skeletal muscle-powered adaptive biological machines, Proc. Natl. Acad. Sci. USA 113 (13) (2016) 3497–3502.
[45] J. Kim, L.J. Cote, F. Kim, J. Huang, Visualizing graphene based sheets by fluorescence quenching microscopy, J. Am. Chem. Soc. 132 (1) (2010) 260–267.
[46] W.C. Ballance, V. Karthikeyan, I. Oh, E.C. Qin, Y. Seo, T. Spearman-White, R. Bashir, Y. Hu, H. Phillips, H. Kong, Preoperative vascular surgery model using a single polymer tough hydrogel with controllable elastic moduli, Soft Matter 16 (34) (2020) 8057–8068.